Particles on Surfaces 8:

Detection, Adhesion and Removal

Editor: *K.L. Mittal*

CRC Press
Taylor & Francis Group

Particles on Surfaces 8: Detection, Adhesion and Removal

Taylor & Francis
Taylor & Francis Group
http://taylorandfrancis.com

Particles on Surfaces 8: Detection, Adhesion and Removal

Editor:
K.L. Mittal

CRC Press
Taylor & Francis Group
Boca Raton London New York

CRC Press is an imprint of the
Taylor & Francis Group, an **informa** business

First published 2003 by VSP Publishing

Published 2018 by CRC Press
Taylor & Francis Group
6000 Broken Sound Parkway NW, Suite 300
Boca Raton, FL 33487-2742

© 2003 by Taylor & Francis Group, LLC
CRC Press is an imprint of Taylor & Francis Group, an Informa business

No claim to original U.S. Government works

ISBN 13: 978-90-6764-392-4 (hbk)

This book contains information obtained from authentic and highly regarded sources. Reasonable efforts have been made to publish reliable data and information, but the author and publisher cannot assume responsibility for the validity of all materials or the consequences of their use. The authors and publishers have attempted to trace the copyright holders of all material reproduced in this publication and apologize to copyright holders if permission to publish in this form has not been obtained. If any copyright material has not been acknowledged please write and let us know so we may rectify in any future reprint.

Except as permitted under U.S. Copyright Law, no part of this book may be reprinted, reproduced, transmitted, or utilized in any form by any electronic, mechanical, or other means, now known or hereafter invented, including photocopying, microfilming, and recording, or in any information storage or retrieval system, without written permission from the publishers.

For permission to photocopy or use material electronically from this work, please access www. copyright.com (http://www.copyright.com/) or contact the Copyright Clearance Center, Inc. (CCC), 222 Rosewood Drive, Danvers, MA 01923, 978-750-8400. CCC is a not-for-profit organization that provides licenses and registration for a variety of users. For organizations that have been granted a photocopy license by the CCC, a separate system of payment has been arranged.

Trademark Notice: Product or corporate names may be trademarks or registered trademarks, and are used only for identification and explanation without intent to infringe.

Visit the Taylor & Francis Web site at
http://www.taylorandfrancis.com

and the CRC Press Web site at
http://www.crcpress.com

Contents

Preface vii

Part 1: Particle Analysis / Characterization and General Cleaning-Related Topics

The nature and characterization of small particles
R. Kohli 3

Surface and micro-analytical methods for particle identification
D.A. Cole, J. Humenansky, M. Kendall, P.J. McKeown, V. Pajcini and J.H. Scherer 29

The haze of a wafer: A new approach to monitor nano-sized particles
K. Xu, R. Vos, G. Vereecke, M. Lux, W. Fyen, F. Holsteyns, K. Kenis, P.W. Mertens, M.M. Heyns and C. Vinckier 47

Particle transport and adhesion in an ultra-clean ion-beam sputter deposition process
C.C. Walton, D.J. Rader, J.A. Folta and D.W. Sweeney 63

Particle deposition from a carry-over layer during immersion rinsing
W. Fyen, K. Xu, R. Vos, G. Vereecke, P. Mertens and M. Heyns 77

The use of surfactants to reduce particulate contamination on surfaces
M.L. Free 129

The use of rectangular jets for surface decontamination
E.S. Geskin and B. Goldenberg 141

Ice-air blast cleaning: Case studies
D. Shishkin, E. Geskin, B. Goldenberg and O. Petrenko 153

Development of a technique for glass cleaning in the course of demanufacturing of electronic products
E.S. Geskin, B. Goldenberg and R. Caudill 167

Part 2: Particle Adhesion and Removal

Mechanics of nanoparticle adhesion — A continuum approach
J. Tomas 183

A new thermodynamic theory of adhesion of particles on surfaces
M.A. Melehy 231

Particle adhesion on nanoscale rough surfaces
B.M. Moudgil, Y.I. Rabinovich, M.S. Esayanur and R.K. Singh 245

Advanced wet cleaning of sub-micrometer sized particles
R. Vos, K. Xu, G. Vereecke, F. Holsteyns, W. Fyen, L. Wang, J. Lauerhaas, M. Hoffman, T. Hackett, P. Mertens and M. Heyns 255

Modified SC-1 solutions for silicon wafer cleaning
C. Beaudry, J. Baker, R. Gouk and S. Verhaverbeke 271

Investigation of ozonated DI water in semiconductor wafer cleaning
J. DeBello and L. Liu 279

Possible post-CMP cleaning processes for STI ceria slurries
R. Small and B. Scott 293

The ideal ultrasonic parameters for delicate parts cleaning
T. Piazza and W.L. Puskas 303

Effects of megasonics coupled with SC-1 process parameters on particle removal on 300-mm silicon wafers
S.L. Wicks, M.S. Lucey and J.J. Rosato 315

Influences of various parameters on microparticles removal during laser surface cleaning
Y.F. Lu, Y.W. Zheng, L. Zhang, B. Luk'yanchuyk, W.D. Song and W.J. Wang 323

Particle removal with pulsed-laser induced plasma over an extended area of a silicon wafer
T. Hooper, Jr. and C. Cetinkaya 335

Particle removal by collisions with energetic clusters
J. Perel, J. Mahoney, P. Kopalidis and R. Becker 345

Particles on Surfaces 8: Detection, Adhesion and Removal, pp. vii–viii
Ed. K.L. Mittal
© VSP 2003

Preface

This volume documents the proceedings of the 8th International Symposium on Particles on Surfaces: Detection, Adhesion and Removal held under the auspices of MST Conferences in Providence, Rhode Island, June 24–26, 2002. This event represented a continuation of the series of symposia initiated in 1986 under the aegis of the Fine Particle Society. Since 1986 this topic has been covered on a regular biennial basis (except no symposium was held in 1994) and the proceedings of these earlier symposia have been properly documented in six hard-bound books [1–6].

As mentioned in the Preface to the book *Particles on Surfaces 7: Detection, Adhesion and Removal* [6] the study of particles on surfaces is extremely crucial in a host of diverse technological areas, ranging from microelectronics to optics to biomedical. In a world of shrinking dimensions and with the tremendous interest in various nanotechnologies, the need to understand the physics of nanoparticles becomes quite patent. With the interest in and concern with nanoparticles comes the need for new and more sensitive metrological and analysis techniques to detect, quantitate, analyze and characterize very small particles on a host of substrates. Also even a cursory look at the literature will evince that currently there is a high tempo of activity in devising new ways or ameliorating the existing techniques to remove real small particles.

The technical program for this symposium was comprised of 30 papers covering many different aspects of particles on surfaces. It should be mentioned that throughout the symposium there were lively and illuminating discussions and certain areas where an urgent and dire need was felt for intensified R&D efforts were highlighted.

Now coming to this volume, it contains a total of 21 papers covering many ramifications of particles on surfaces. Apropos, this volume also contains a paper which was presented in the earlier symposium but was not published at that time. It must be recorded that all manuscripts were rigorously peer-reviewed and all were revised (some twice or even thrice) and properly edited before inclusion in this volume. Concomitantly, this volume represents an archival publication of the highest standard. It should not be considered a proceedings volume in the usual sense, as many proceedings volumes are neither peer-reviewed nor adequately edited.

This volume is divided into two parts: Part 1: Particle Analysis/Characterization and General Cleaning-Related Topics; and Part 2: Particle Adhesion and Removal. The topics covered include: nature and characterization of small particles;

surface and micro-analytical methods for particle identification; haze as a new method to monitor nano-sized particles; particle transport and adhesion in ion-beam sputter deposition process; particle deposition during immersion rinsing; ice-air blast cleaning; rectangular jets for surface decontamination; factors important in particle adhesion and removal; mechanics of nanoparticle adhesion; particle adhesion on nanoscale rough surfaces; various techniques for cleaning or removal of particles from different substrates including wet cleaning, use of modified SC-1 solutions, use of surfactants, ozonated DI water, ultrasonic, megasonic, laser, energetic clusters; and post-CMP cleaning.

Yours truly sincerely hopes that this volume and its predecessors [1–6] would be of immense value to anyone interested in the world of particles on surfaces, and these volumes collectively would serve as a resource for information on contemporary R&D activity in this extremely technologically important area.

Acknowledgements

This section is always the pleasant part of writing a Preface. First, I am thankful to Dr. Robert H. Lacombe, a dear friend and colleague, for taking care of the organizational aspects of this symposium. Special thanks are due to the reviewers for their time and efforts in providing many valuable comments which are a prerequisite for a high standard publication. The authors must be thanked for their interest, enthusiasm and contribution which were essential ingredients in making this volume a reality. Finally my sincere appreciation goes to the staff of VSP (publisher) for materializing this book.

K.L. Mittal
P.O. Box 1280
Hopewell Jct., NY 12533

1. K.L. Mittal (Ed.), *Particles on Surfaces 1: Detection, Adhesion and Removal.* Plenum Press, New York (1988).
2. K.L. Mittal (Ed.), *Particles on Surfaces 2: Detection, Adhesion and Removal.* Plenum Press, New York (1989).
3. K.L. Mittal (Ed.), *Particles on Surfaces 3: Detection, Adhesion and Removal.* Plenum Press, New York (1991).
4. K.L. Mittal (Ed.), *Particles on Surfaces: Detection, Adhesion and Removal.* Marcel Dekker, New York (1995). (Proceedings of the 4th Symposium.)
5. K.L. Mittal (Ed.), *Particles on Surfaces 5&6: Detection, Adhesion and Removal.* VSP, Utrecht (1999). (Proceedings of the 5th & 6th Symposia.)
6. K.L. Mittal (Ed.), *Particles on Surfaces 7: Detection, Adhesion and Removal.* VSP, Utrecht (2002).

Part 1

Particle Analysis / Characterization and General Cleaning-Related Topics

Taylor & Francis
Taylor & Francis Group
http://taylorandfrancis.com

Particles on Surfaces 8: Detection, Adhesion and Removal, pp. 3–28
Ed. K.L. Mittal
© VSP 2003

The nature and characterization of small particles

RAJIV KOHLI*

Maxor Corporation, 2452 Clover Basin Drive, Longmont, CO 80503, USA

Abstract—Nanosize particles are of fundamental and practical interest for advanced materials and devices. As feature sizes shrink, nanoparticle contamination will also become increasingly important and will present an ongoing challenge to achieve and maintain high product yields. In order to employ appropriate material and product development strategies, or preventive assembly and remediation strategies to control nanoparticle contamination, it is necessary to understand the nature of nanosize particles and to characterize these particles. Particles in the size range 0.1 nm to 100 nm present unique challenges and opportunities for their imaging and characterization. Critical information for this purpose is the number and size of the particles, their morphology, and their physical and chemical structure. A brief review of the nature of small particles is presented. Emerging techniques for characterizing particles, such as scanning near-field optical microscopy (SNOM), hot electron microcalorimetry, multiphoton microscopy and Raman chemical imaging, are briefly described.

Keywords: Small particles; characterization; innovative imaging techniques; SNOM; atom probe; HAADF-STEM; Raman microscopy; multiplexed multiphoton microscopy (MMM).

1. INTRODUCTION

Small particles in the submicrometer and subnanometer size range are of fundamental interest in a wide variety of industries. The development of advanced nanomaterials and nanodevices involves the efficient application of nanometer size particles. By contrast, nanometer size particles as contaminants are a leading cause of failure of components and end products in widely diverse industries, such as electronics, semiconductors and optics. For example, in the data storage industry, minimizing contaminant particles on hard disk drive components is critical to drive performance and high product yield. The current nominal flying height at which the head flies over the disk is 17 to 25 nm which will be even lower in future product designs. If a particle of similar dimensions is trapped between the head and the disk, it can cause a catastrophic failure of the drive [1].

*Present address: RKAssociates, 2450 Airport Road, #D-238, Longmont, CO 80503, Phone: (1-303) 682-3217, E-mail: kohlirkassoc@hotmail.com

In order to continuously advance material developments, or to develop remediation strategies to minimize or eliminate contaminant particles from the manufacturing process, it is necessary to understand the interactions of nanometer size particles. This, in turn, requires detailed characterization of these particles. As the particle size becomes smaller, high-resolution qualitative and quantitative methods are required to measure and physically and chemically characterize these particles. A number of methods have been developed for imaging and characterizing particles from micrometer size to the atomic scale [2-7]. These methods take advantage of the complete range of properties of the materials. Many of these methods are commercially available, while other methods have been successfully demonstrated. Here we discuss recent developments and applications of selected less-common methods that hold tremendous promise for imaging, physical characterization and chemical analysis of nanometer and subnanometer-size particles.

2. NATURE OF SMALL PARTICLES

2.1. Sizes of small particles

In referring to small particles, the size of the particles can be discussed in terms of various physical phenomena. For example, the interactions of particles much larger than 1 μm in diameter are increasingly dominated by gravitational forces, while van der Waals and other forces tend to dominate their interactions below that size. Particles with diameters of 0.3 to 0.7 μm are of the same size as the wavelength of visible light, which is the limit of resolution (Abbe diffraction limit) in conventional optical microscopic observation of particles of that size. However, as we shall see in Section 3.3.4, scanning near-field optical microscopy makes it now possible to bypass the Abbe diffraction limit to resolve particles as small as 30 nm.

Particles in the size range 20 to 100 nm are referred to as ultrafine, while nanometer size particles have diameters smaller than 20 nm. Due to the need to understand aerosol behavior, two additional classes of particle sizes have been defined. Very small particles refer to particles smaller than 5 nm, while molecular size defines particles with diameters smaller than 1 nm [8].

2.2. Particle interactions

The physical nature of very small particles (<20 nm) cannot be thought of in terms of classical surface or volume continua. Rather, the molecules statistically associated with the particle will tend to define their physical and chemical interactions. As Table 1 shows, the number of molecules associated with a particle increases with increasing particle size, but the fraction of the molecules at the surface decreases with increasing particle size. For a particle of 20 nm diameter, the number of molecules at the surface is only about 12%, but the number is nearly 90% for a particle of 2 nm diameter. Consequently, the overall behavior of very

small particles is governed by the surface and binding energies of the molecules in the particle. These particles are neither solid nor liquid, and do not behave like individual molecules. Such particles are regarded as a complex structure whose behavior depends on the positions of the individual molecules and the combined electronic charge distribution [9, 10].

Table 1.
Characteristics of molecules associated with very small particles

Particle size (nm)	Cross-sectional area (10^{-18} m^2)	Mass (10^{-25} kg)	Number of molecules	% of molecules at the surface
0.5	0.2	0.65	1	–
1.0	0.8	5.2	8	100
2.0	3.2	42	64	90
5.0	20	650	1×10^3	50
10.0	80	5.2×10^3	8×10^3	25
20.0	320	4.2×10^4	6.4×10^4	12

Only simple interactions of very small particles are presently well understood. Due to the technological importance of very small particles in advanced materials and nanotechnology, advances in kinetic theory, solid state chemistry, quantum mechanics and aerosol dynamics are essential to better understanding of particle interactions. Combined with the very high spatial resolution and chemical composition capabilities of newer characterization techniques, it will be possible to predict the behavior of very small particles in complex systems in the future. In turn, these predictions will provide the basis for understanding the transport, adhesion and detachment of these particles in real systems, as well as making it possible to design materials with specific properties. One example is the recent synthesis of monodisperse Fe-Pt nanoparticles of controlled size (3-10 nm) and composition to yield chemically and mechanically robust ferromagnetic nanocrystal assemblies for very high areal density magnetic recording (terabits per unit area) [11].

2.3. Elucidating the fundamental interactions of very small particles

One major source of particles is chemically-induced transformation of gaseous matter into particles. These particles can subsequently grow by condensation and coagulation into larger particles at a growth rate that depends on factors such as particle size and concentration [12-14]. This gas-to-particle transformation is important for assembly processes in which gaseous precursors such as acid gases are present, or for products that employ volatilizable materials, such as motor bearing grease and lubricants. The understanding of gas phase reactions in the formation of particles has advanced considerably, but important chemical and physical mechanisms are still unresolved, particularly for particles smaller than 10 nm size.

As noted earlier, such particles have to be considered as complex structures whose properties and interactions are determined by the number and position of the molecules on the surface. In fact, the interactions of these particles will be largely between the molecules at the surface, which are, in turn, determined by atomic, electronic and nuclear motions. These interactions typically occur on timescales of picoseconds (10^{-12} s) to subzeptoseconds (10^{-21} to 10^{-22} s). For example, subpicosecond X-rays or electrons [15, 16] or femtosecond pulsed lasers [17] can probe events such as creating and breaking of chemical bonds, while attosecond pulses [18-20] can be used to study the motions of electrons that bind atoms together. The motions of nuclei within the electrons happen on an even briefer timescale and the recently proposed source of zeptosecond laser pulses should help to illuminate strong nuclear interactions [21].

3. MEASUREMENT AND CHARACTERIZATION OF PARTICLES

3.1. Sizing and classification

Several techniques are available to count, size and classify single ultrafine particles as small as 2 nm in diameter [13, 14]. For example, the ultrafine condensation nucleus counter can detect particles down to 3 nm with a counting efficiency of >70%, while differential mobility size spectrometry can provide size distribution of particles in the <1 to 200 nm range [22-30]. Recently, the first condensation nucleus counter (CNC) capable of detecting individual ions has been developed [31]. However, many of these methods do not provide any information on the size distribution of individual particle types. To overcome these limitations, an on-line, semicontinuous double size spectrometry method has been developed to provide size and effective density of single particles in the range 3 to 50 nm [32]. In this method, particles in a narrow size range are selected by an electrical mobility size classifier and then resized by a hypersonic impactor [33, 34]. The first step selects the particles by their Stokes diameter, which is the geometric diameter of spherical particles. The second step sizes the singly-charged particles by their aerodynamic diameter, which is dependent on the particle mass as well as the Stokes diameter. The impactor flow is supersonic and the particle capture is measured by an electrometer. The collection efficiency of the impactor is better than 80% for particles down to 3 nm diameter.

Most differential mobility size spectrometry instruments are designed to operate at ambient pressure for probing aerosol particles in the atmosphere. By contrast, in semiconductor fabrication contamination from nanometer-sized particles formed at low pressures can lead to significant yield loss [35]. In response, differential mobility analyzer instruments have been developed for low-pressure operation [36, 37]. These instruments employ larger diameter and longer connecting tubes between the instrument and the vacuum pumps, together with mass flow controllers especially designed for low pressures. These features ensure a low

pressure drop and a large evacuation capacity. The instrument has successfully demonstrated accurate mobility classification of particles in the size range 6-12 nm at pressures as low as 200 Pa, approaching the operating pressures in semiconductor fabrication.

3.2. Particle analysis

The chemical composition of nanosize particles is important information needed to develop a complete understanding of the behavior of these particles. Traditionally, the particles are collected by one or more of the available sampling methods on a filter, substrate or grid located in an impactor and analyzed using off-line techniques, such as electron microscopy and vibrational and mass spectroscopy [2, 30, 38, 39]. One method that is increasingly used for offline analysis of individual particles is laser microprobe mass spectrometry (LMMS). The particles are irradiated with a high power pulsed laser and the fragments are analyzed by mass spectrometry [40, 41]. LMMS can detect trace metals, inorganic compounds, and organic compounds in individual particles [42-45]. However, because it is an offline technique that requires the particles to be exposed to a vacuum, the particle composition can be affected. In addition, there is a significant time delay in returning data because the samples must be analyzed in a remote laboratory.

3.2.1. Single particle analysis

Recently, a number of instruments have been developed for on-line collection and analysis of single aerosol particles in real time [30, 46-48]. In these instruments, the particles are aerodynamically sized followed by chemical analysis by mass spectrometric methods to obtain information about molecules and not just elements. The particles are desorbed and ionized in the source region of the mass spectrometer. Ionization can be achieved by non-laser thermal vaporization [49-52] and analyzed by a magnetic sector mass spectrometer or by a quadrupole mass spectrometer [53], or an ion trap [54, 55]. Alternatively, particles can be ionized chemically [56-58], by electron impact [39, 53], or by laser vaporization [59-65]. Aerosol time-of-flight mass spectrometry (ATOFMS) has been successfully demonstrated in a field-transportable instrument for real time on-line analysis of single aerosol particles down to 0.1 μm [59-62].

These real-time instruments have been successfully demonstrated to also provide information on multicomponent crystallization [66], compound speciation [67], surface coatings [68] and even the oxidation state of particles [69].

3.2.2. High-resolution X-ray spectroscopy

Semiconductor energy-dispersive spectrometers (EDS) and wavelength-dispersive spectrometers (WDS) are commonly employed as analytical tools for off-line chemical identification of particles, but these detectors cannot resolve closely-spaced or overlapping X-ray peaks in complicated spectra. For example, the severe peak overlaps between the Si K_α and the W M_α X-ray lines prevent their identification by semiconductor EDS [70]. High-resolution X-ray detectors are

required to meet the analysis requirements for small particles, particularly particles with a diameter <0.1 μm.

The leading techniques for developing high-resolution detectors are based on the use of semiconductor thermistors, superconducting edge transition detectors, superconducting tunneling junctions, and magnetic calorimeters [71-75]. With these methods it is possible to obtain an energy resolution of 3 to 13 eV full width at half maximum (FWHM) that is an order of magnitude better than the resolution obtainable with semiconductor EDS (~ 130 eV at FWHM) and is comparable to semiconductor WDS (~ 2 to 20 eV at FWHM).

Of the techniques mentioned above, the superconducting edge transition detector has been most often applied for particle analysis. In a typical configuration of such a detector system, also referred to as microcalorimeter EDS, there is a metal film to absorb the X-rays, a thermometer to measure the temperature of the electrons in the absorber, and a coupling to a heat sink (Fig. 1).

When a particle or a photon interacts with the absorber, the incident energy is converted to heat. The corresponding temperature rise is measured by a superconductor tunnel junction that is cooled to well below the phase transition temperature. The amplitude of the current pulse through the junction is directly proportional to the incident energy. The fundamental energy resolution limit of these detectors is of the order of 1-3 eV, depending on the absorber material. Present detector technology has achieved a resolution of 3-7 eV, which makes these de-

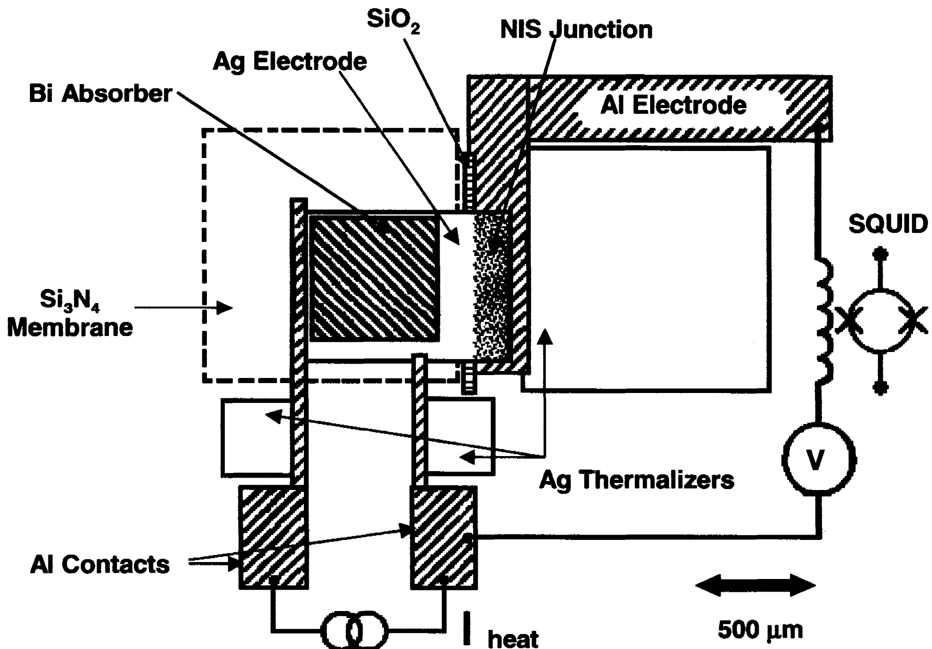

Figure 1. Schematic of a typical microcalorimeter EDS system.

vices very well suited to high-resolution X-ray detection. For example, with a 0.3 μm W particle on a Si substrate it was possible to resolve the M_α, M_β, M_γ and the M_ζ peaks for W using microcalorimeter EDS (Fig. 2). Similar results were obtained on a TiN sample. The L_α peak, both L_β peaks and even the L_η peak for Ti was clearly resolved [70].

Microcalorimeter EDS offers one additional advantage. With its high-energy resolution, all peak shapes and integrated peak intensities are accessible, making it possible to measure chemical shifts in the X-ray spectra. This can provide chemical binding state information [70].

3.2.3. Laser-induced breakdown spectroscopy

Laser-induced breakdown spectroscopy (LIBS) is an atomic emission spectroscopic technique in which successive nanosecond laser pulses ablate a small amount of material from the surface [76-79]. The resulting microplasma emits fluorescence radiation from excited atoms and/or ions that is characteristic of the

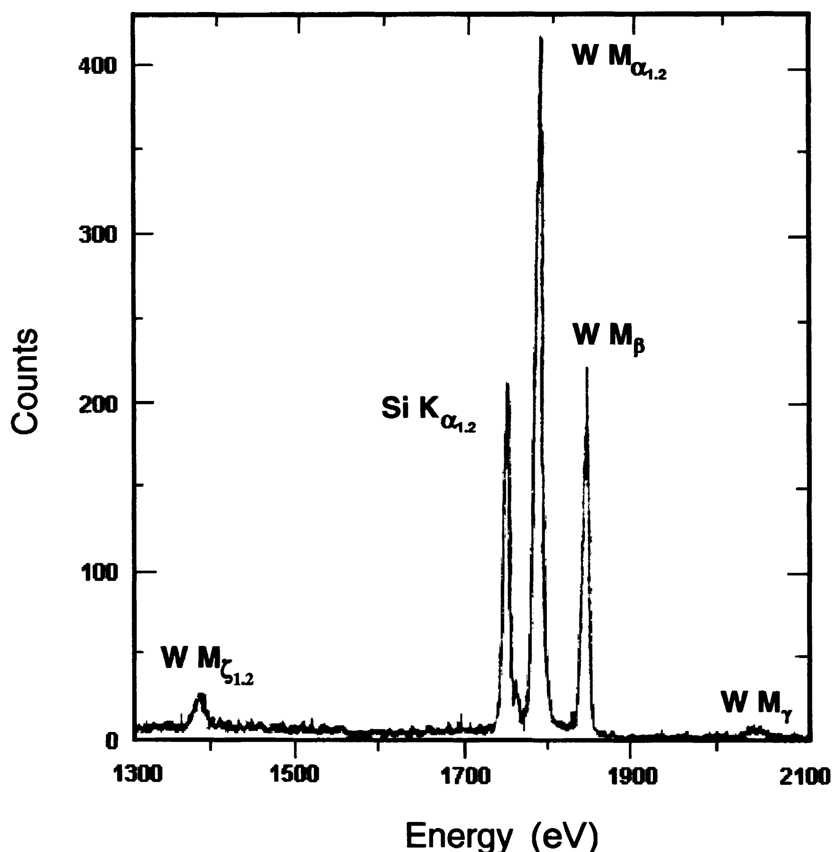

Figure 2. Microcalorimeter EDS spectrum of a tungsten particle on a silicon substrate (courtesy of National Institute of Standards and Technology, Boulder, CO, USA).

elements in the sample. If the same point is ablated successively, the LIBS spectra provide *in situ* cross-sectional analysis of the material. Raman microscopy can achieve very high spatial resolution (~ 1 μm), which gives spectra largely free of contamination from surrounding material. By combining these techniques, elemental analytical data and the chemical composition of the material of interest can be obtained *in situ*. The advantages of combining Raman microscopy with LIBS to identify and analyze pigment particles in artworks have been demonstrated recently [80]. It was determined that the original white paint on a Byzantine icon was $2PbCO_3 \cdot Pb(OH)_2$, but that the subsequent restorative work used ZnO paint.

The LIBS technique can also yield information simultaneously on the size, number density, mass and composition of a wide range of particles, including metal hydrides, coal particles, halons, and elements (As, Be, Fe, Mn, Ni and others). Particles as small as 175 nm have been successfully measured, corresponding to an absolute detectable mass of the order of 10^{-15} g [77]. This shows the very high sensitivity of the LIBS technique for particle characterization.

By combining LIBS with scanning near-field optical microscopy (SNOM), it is possible to map and correlate elemental chemical composition of surfaces with the surface topography [81]. In this method, surface topography is first mapped by scanning the surface with the SNOM probe. The probe is then positioned over a feature of interest, such as a surface contaminant particle, which is vaporized by a laser pulse. Optical emissions from the resulting plasma plume are analyzed to obtain LIBS spectra.

3.3. Particle imaging techniques

3.3.1. Scanning transmission electron microscopy

High-resolution electron microscopic techniques have been developed in response to the need to understand the fundamental properties of nanosize particles. This includes chemical, structural and morphological information of particles.

A very attractive feature of recent scanning transmission electron microscopy (STEM) instruments is the ability to form an electron probe with diameters down to 0.3 Å using aberration correction of the electron lenses [4, 82, 83]. This is achieved with a field-emission gun that provides the signal strength to view and record images, spectra and electron diffraction patterns. In addition, there are a great variety of available detectors that have been developed to simultaneously collect imaging and analytical signals in dedicated STEM instruments (Fig. 3). This makes the STEM an exceptional nanoanalytical tool that can provide detailed information on composition, electronic and crystal structure with atomic resolution and sensitivity [82].

By collecting high-angle annular dark-field (HAADF) images, information about structural variations across the sample can be obtained at the atomic level. Electron energy-loss spectroscopy (EELS) and X-ray energy dispersive spectroscopy (XEDS) provide quantitative data on elemental composition, electronic

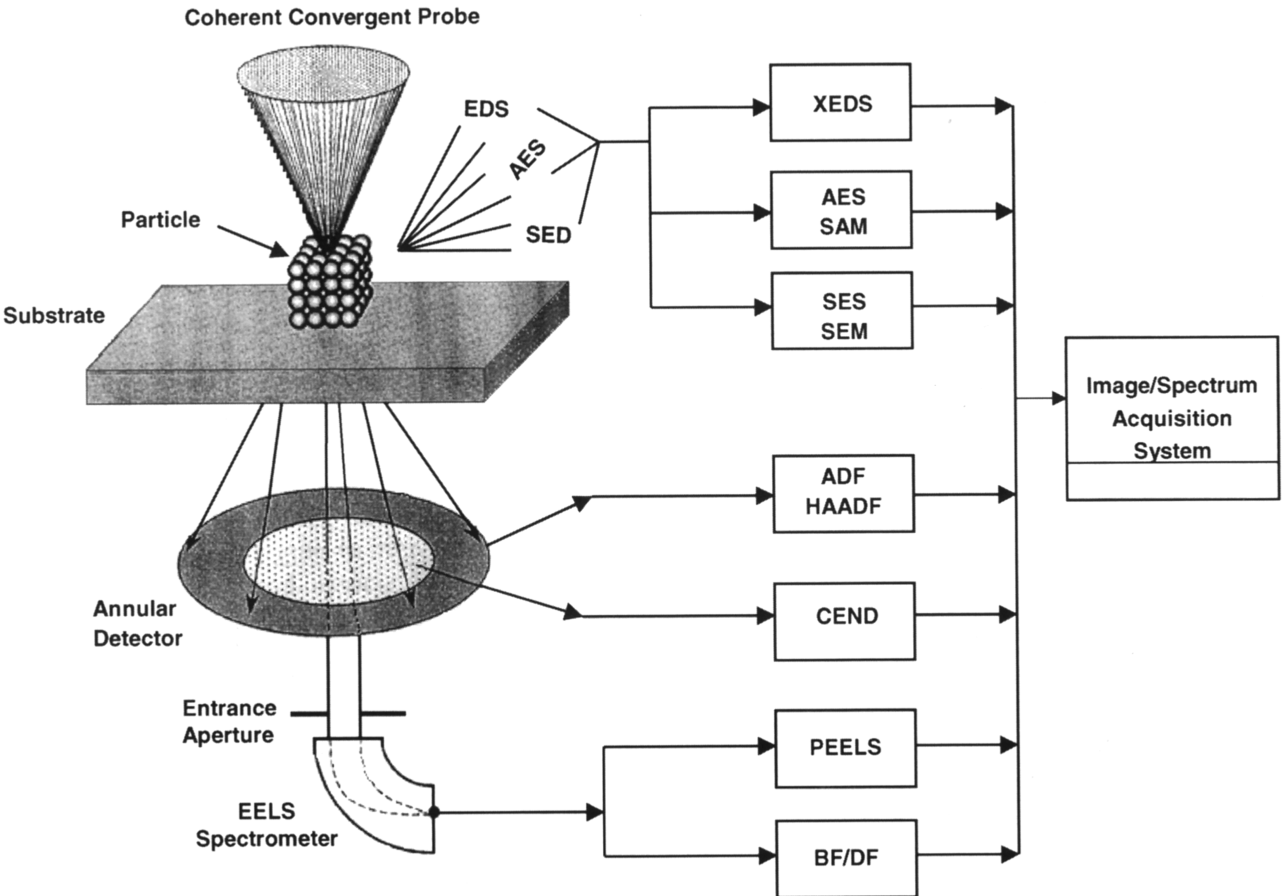

Figure 3. Imaging and analytical modes in the scanning transmission electron microscope.

structure or oxidation state of the sample. In fact, work has been recently reported on the distribution and unambiguous identification of individual gadolinium atoms inside a chain of endohedral Gd-metallofullerenes separated by 1 to 2 nm [83]. Surface topography or surface chemistry of nanoparticles can be obtained by secondary electron spectroscopy (SES) or Auger electron spectroscopy (AES). Nanodiffraction patterns can be acquired from individual nanoparticles to provide information on their crystallographic structure, as well as their structural relationship with the surrounding material, and perhaps also the morphology of the particles.

The resolution of STEM images is determined primarily by the incident probe size, the stability of the microscope, and the inherent properties of the signal generation process. Modern high-resolution microscopes can provide point resolution of 1.3-1.7 Å, although recently lattice imaging has been demonstrated at 0.75-0.89 Å [84, 85] with aberration correction. This level of resolution can be exploited to obtain direct structural information on wide band gap materials at a monoatomic level, such as the 60^0 dislocation in Si-Ge/Si structures [86]. In addition, by using the microscope as a quantitative measuring instrument employing quantitative statistical experimental design, it is possible to measure atom positions with a precision of the order of 0.01 Å [87]. At this level of precision, highly refined solid state theoretical calculations can be made and validated to predict from first principles the exact properties of materials and the interactions between materials.

3.3.2. High-angle annular dark-field (HAADF) STEM imaging

For true quantitative 3D analysis, a single projection of 2D images will not be adequate for a complete description of the object being examined in a STEM. It is necessary to turn to tomography to reconstruct the 3D object from a tilt series of 2D projections. The most common mode of electron tomography is conventional coherent bright field (BF) TEM. However, for crystalline particle imaging and analysis, diffraction (and Fresnel) contrast makes reconstruction of the structure from coherent signals problematic. Other (incoherent) signals must be used that are insensitive to diffraction contrast to reduce or eliminate such problems. High-angle annular dark-field (HAADF) imaging in the STEM does provide images of high compositional contrast, shows little or no diffraction effects, and in which the signal is approximately proportional to the square of the atomic number Z. This is the reason it is also known as 'Z-Contrast' imaging [82, 88-93].

HAADF images are formed by collecting high-angle (typically a few degrees or more) scattered electrons with an annular dark-field detector in dedicated STEM instruments. The images originate from interaction with atomic nuclei and are therefore sensitive to differences in atomic number. The contrast of HAADF images is

- strongly dependent on the average atomic number of the scatterer encountered by the incident probe;
- not strongly affected by dynamical diffraction effects;
- not strongly affected by defocus; and

- not strongly affected by sample thickness variations. Spatial resolution is limited by the size of the focused incident probe.

The spatial resolution and field of view of HAADF STEM imaging complement perfectly the ultra-high-resolution technique of atom probe tomography and the much lower resolution X-ray micro-tomography.

In commercial microscopes, the HAADF signal can be detected very simply by lowering the camera length to values of around 100 mm or less. Both BF (transmitted beam) and dark field (diffracted beam) electrons then fall on the central BF-STEM detector, while the HAADF electrons fall on the annular dark-field detector. Typical HAADF acceptance angles are 2.5 to 6 degrees. HAADF images can be obtained at the same resolution as STEM BF and DF images (atomic resolution with a field emission gun). The specimen must be thin (<40 nm) for most high-resolution imaging applications.

The HAADF technique does have some limitations:

- HAADF imaging is only quasi-spectroscopic;
- the image resolution is not as high as that of HREM images;
- thick specimens cause beam broadening and degradation of the spatial resolution; and
- HAADF images have a much poorer signal-to-noise ratio compared to HREM images.

The HAADF technique shows great promise for very high-resolution analysis. For example, STEM images of a Pt catalyst on a Al_2O_3-Ce_2O_3 support are shown in Fig. 4. The dark round features in the BF image can be either ceria or platinum grains. Only the HAADF image clearly shows the platinum crystals.

There are two potential sources of artefacts in the HAADF technique:

1. HAADF imaging is more strongly dependent on thickness of the specimen than back-scattered electron imaging. Specimens with strong thickness variations may show high intensity in thicker areas. In such specimens, the HAADF signal is not necessarily indicative of high atomic number.
2. Structures such as dislocations may show up strongly in HAADF images without any local concentration of high-atomic number material. Small changes in crystal tilt will normally lead to strong changes in dislocation contrast, similar to the effect seen in TEM BF and DF images.

3.3.3. Field-emission environmental SEM

The field-emission environmental scanning electron microscope (FE-ESEM) is an instrument with unique capabilities [94, 95]. In conventional scanning electron microscopy a relatively high vacuum in the specimen chamber is required to prevent atmospheric interference with the primary or secondary electrons. By contrast, nonconductive and uncoated specimens can be examined in an FE-ESEM at high chamber pressure (10 Pa to 1.33 kPa) and temperatures up to 1273 K. Since the residual gas pressure range in the specimen chamber can exceed saturated wa-

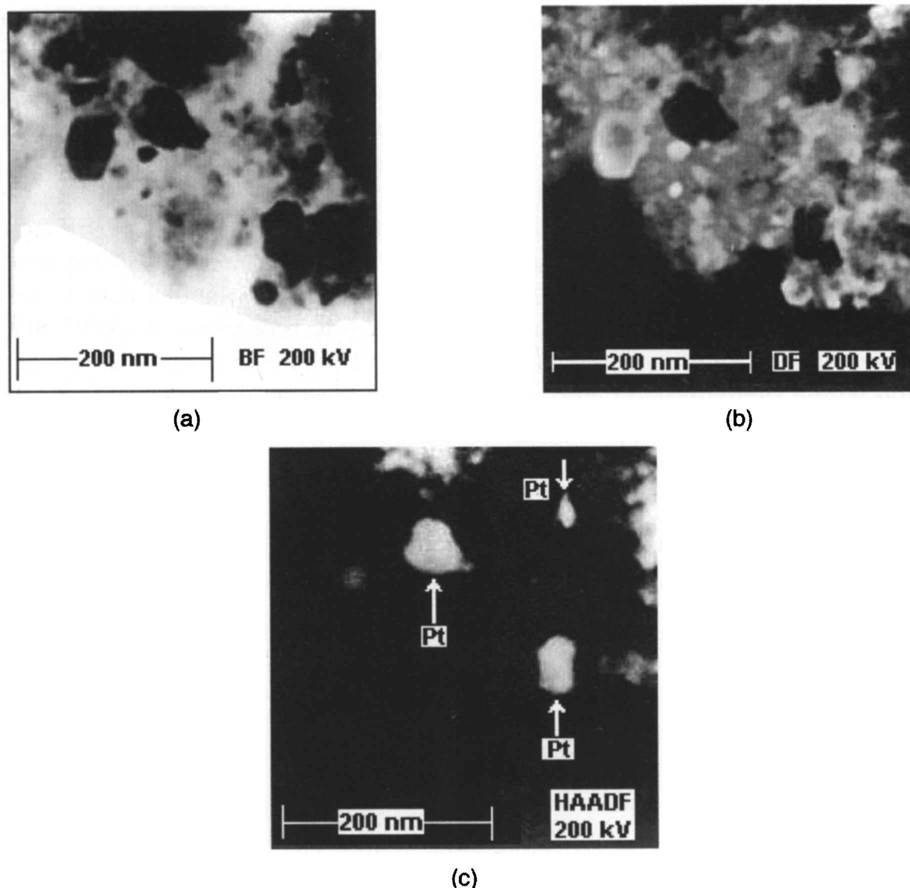

Figure 4. STEM images of an aged platinum catalyst on Al_2O_3-Ce_2O_3 support. (a) BF image; (b) DF image; (c) HAADF image (courtesy of FEI Company, Portland, OR, USA).

ter vapor pressure, water-containing specimens can be imaged without drying out. In such "wet mode" imaging, the specimen chamber is isolated from the rest of the vacuum system.

When the electron beam (primary electrons) ejects secondary electrons from the surface of the sample, the secondary electrons collide with water molecules, which, in turn, function as a cascade amplifier, delivering the secondary electron signal to the positively biased gaseous secondary electron detector. The water molecules are positively ionized, and thus they are attracted toward the specimen, serving to neutralize the negative charge produced by the primary electron beam. The applied accelerating voltage can be matched to the required edge and penetration effects, while the gas pressure can be varied to remove all specimen charging. The field-emission gun produces a brighter filament image (primary electron beam) than either tungsten or lanthanum hexaboride (LaB_6) sources, and the ac-

celerating voltage may be lowered significantly, permitting nondestructive imaging of fragile specimens.

The key benefits of the FE-ESEM imaging technique are listed below:

- True secondary electron imaging at high chamber pressure (to 1330 Pa);
- no charging of non-conductive samples;
- low-*Z* materials can be observed;
- contaminated samples can be observed;
- porous material can be imaged;
- hydrated samples remain fully stable; and
- no coating interference.

There are two important benefits in X-ray analysis with the FE-ESEM of uncoated specimens.

1. No X-ray lines from the coating interfere with the characteristic X-ray spectrum generated in the specimen. The absence of conductive coatings rids the potential absorption and interference artefacts.
2. X-ray analysis can be performed at high accelerating voltages. No charging artefacts are observed which allows the operator to choose any acceleration voltage for optimal X-ray analysis.

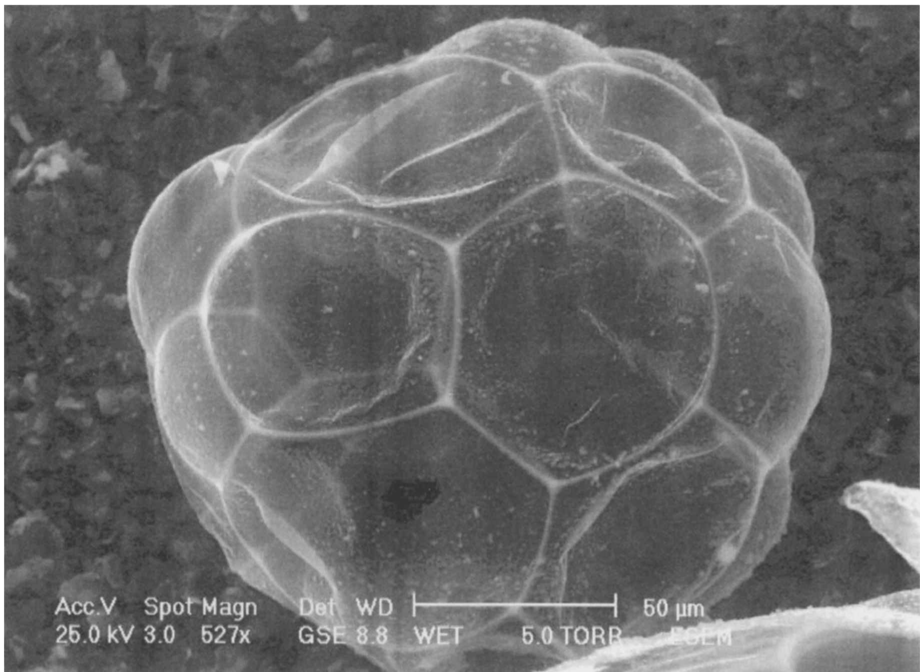

Figure 5. Image of a diesel exhaust particle at approximately 650 Pa chamber pressure in an FE-ESEM (courtesy of FEI Company, Portland, OR, USA).

This combination of characteristics makes the FE-ESEM ideal for obtaining high magnification secondary electron images of low atomic number materials in their uncoated, natural and stable state (Fig. 5).

3.3.4. Scanning near-field optical microscopy (SNOM)

The key requirements for characterizing nanometer-scale objects are high sensitivity and high spatial resolution. Although scanning tunneling microscopy (STM) and atomic force microscopy (AFM) provide exceptional spatial resolution of the order of 1 nm or less, neither technique provides chemical identification of surface species. The reason for this is that in STM and AFM only the outer electrons of the surface atoms are involved in the interactions of the probe tip with the surface. No spectroscopic information is obtained from the inner shell structure of the atom. Recently, an infrared AFM has been developed and successfully demonstrated as described in Section 3.3.9.

Scanning near-field optical microscopy (SNOM) can meet both these requirements of high sensitivity and high spatial resolution [96-99]. Its unique advantage is the existence of a spatial dimension that makes it possible to perform chemical identification. From theoretical considerations, the fundamental optical diffraction limit of resolution is given by $0.61\lambda/n\sin\theta$, where λ is the wavelength of the employed light and $n\sin\theta$ is the numerical aperture [100]. This limits the resolution to approximately 250-400 nm for visible light. SNOM overcomes the Abbe diffraction limit in the optical regime by scanning a nanometer-sized aperture probe (50-100 nm) in close proximity (1-15 nm) to the sample surface. As a result, the light is concentrated as a subwavelength source that also acts in the optical near field.

A commercial SNOM system consists of one or more optical microscopes for reflection or transmission mode operation; the SNOM stage with the scanner and the SNOM sensor module with a shear force detector; the SNOM control unit with the laser and associated optics; and a software control system for fine positioning and automated operation. Most commonly, the SNOM probe tip is maintained at a constant distance from the sample surface by optical detection of the damping of an oscillating probe tip by shear force. Non-optical distance controls have also been implemented [96-99].

Tapered aperture probes with effective aperture sizes of 50-100 nm are routinely fabricated by adiabatic pulling of optical fibers during heating with a laser [101]. Alternatively, the probe tip can be fabricated by etching glass fibers at the tip [102], or by tube etching [103]. Tube etching produces very smooth probe tips with no pinholes and with optical transmission coefficients of 10^{-3} compared with 10^{-5}-10^{-6} for pulled fiber tips [104]. The probe is coated with a thin metallic film of aluminum to concentrate the light within the probe. The effective aperture size that can be achieved with aperture probes is 8-10 nm, which may be the practical limit of spatial resolution with these probes because of the finite skin depth of real metals, although a spatial resolution of ~ 5 nm has been reported [105]. One of the best optical metals is aluminum for which the penetration depth is ~ 8 nm for green light.

Other methods for fabricating aperture probes include focused ion-beam milling [106] and microfabrication [107, 108]. These methods would make it possible to fabricate inexpensive and highly reproducible probes. Using a microfabricated silicon cantilever probe with a quartz tip, a FWHM (full width at half maximum) resolution of 32 nm has been demonstrated [107].

A high resolution SNOM image of a sample of a polymer is shown in Fig. 6. The diameter and the depth of the pit are 100 nm and 5 nm, respectively. Judging from the width of the edge of the pit, the lateral resolution of the SNOM image is about 10 nm and the vertical resolution is about 1 nm (T. Kataoka, personal communication).

To overcome the limitations of aperture probes, an apertureless SNOM technique has been demonstrated in which a sharp vibrating tip is used to scatter the near field of the sample to achieve spatial resolution of 1 nm [109]. However, in this configuration the resolution is limited by the radius of curvature of the tip itself. By replacing the physical aperture with a nanoscopic active medium that acts as a light source, such as dye molecules, quantum dots, or diamond color centers, single-molecule resolution can be achieved [110].

Specific chemical information has been successfully obtained by combining SNOM with experimental methods such as cathodiluminescence [96], infrared spectroscopy [111-113], surface-enhanced Raman spectroscopy [99, 114, 115] and fluorescence imaging [99, 115, 116]. SNOM has also been combined with laser-induced breakdown spectroscopy in a single instrument to achieve spatially-

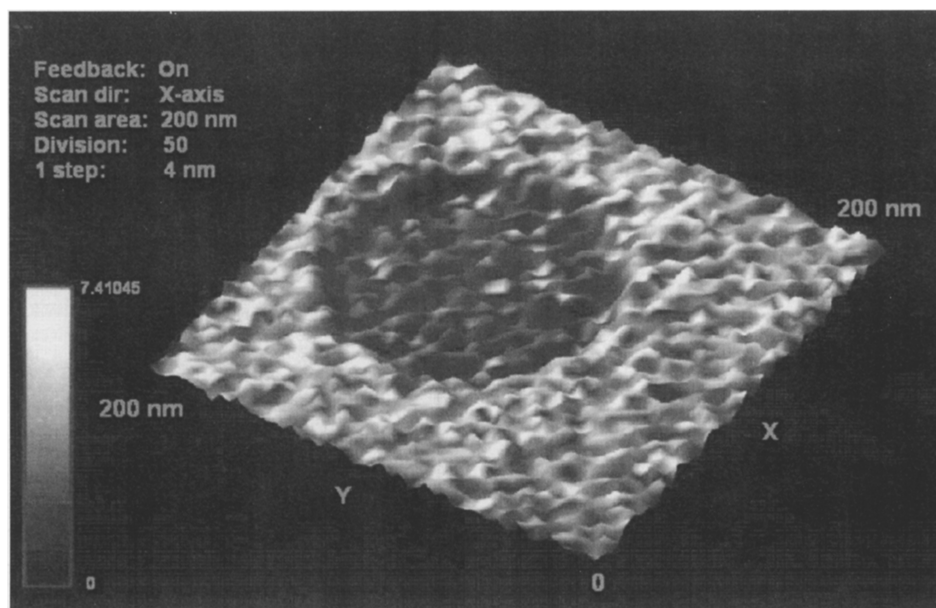

Figure 6. The SNOM image of a pit in a polymer sample (courtesy of Osaka University, Osaka, Japan).

resolved chemical imaging of surface particles [81]. Recently, nanoscale atmospheric pressure laser ablation mass spectrometry has been demonstrated at a spatial resolution of less than 200 nm [117].

Figure 7 shows SNOM images of bacteria bred to produce green fluorescence protein. In transmission mode, the location of the fluorescent protein is clearly distinguished. The origin of the fluorescent light is approximately 20 nm below the surface of the bacterium.

Recent information on SNOM and its wide range of applications for particle imaging and analysis can be found in several publications [96-99].

3.3.5. Three-dimensional atom probe imaging

The 3-dimensional atom probe (3DAP) is a quantitative technique that provides atomic scale 3-dimensional elemental maps of atoms within a volume 20 nm × 20 nm × 100 nm of a conductive sample [118, 119]. As with the STM, a single atom and its neighbors can be imaged. However, 3DAP provides two major advantages over the STM:

- Elemental analysis in which each single atom is chemically identified by time-of-flight; and
- position-sensitive detection, which makes the chemical map of the atoms truly three dimensional.

In a typical 3DAP system, single atoms are field evaporated from a needle-shaped sample mounted on a cryogenically-cooled goniometer (Fig. 8). Atoms are ionized from the surface under a very high electric field and projected toward a position-sensitive detector placed at a distance of 250 to 650 mm from the sample. Ionization occurs from the surface of the specimen regularly, which makes it possible to ionize atoms by atomic layer, as well as by atomic order, thereby achieving atomic layer resolution. Atoms are chemically identified by time-of-flight mass spectrometry. The detector gives an accurate measurement of the ion impact positions and masses. The very high magnification of the instrument yields highly accurate (0.2 nm) impact coordinates, from which the original positions of the atoms at the tip surface are derived. Modern 3DAP instruments are equipped with a reflectron energy compensator, and are able to achieve a mass resolution, m/Dm, larger than 300 [118]. With this performance, most of the alloying elements contained in complicated nanocrystalline alloys can be identified without any ambiguity.

An example of element and concentration mapping obtained by a 3DAP is shown in Fig. 9. In the elemental map of the omega phase precipitated in an aged Al alloy, individual Al, Cu, Mg and Ag atoms are shown [120]. By counting the number of atoms in each pixel, the elemental map can be converted to a concentration profile. 3DAP gives very accurate compositional information on the interface of nanosized particles embedded in a matrix phase. This type of analysis is impossible with an analytical transmission electron microscope because the typical thin foil thickness of TEM specimens is larger than 200 nm. If the particles embedded in the matrix are smaller than the thickness of the sample, the EDS spectra obtained from the nanosized particles will always be influenced by the surrounding matrix.

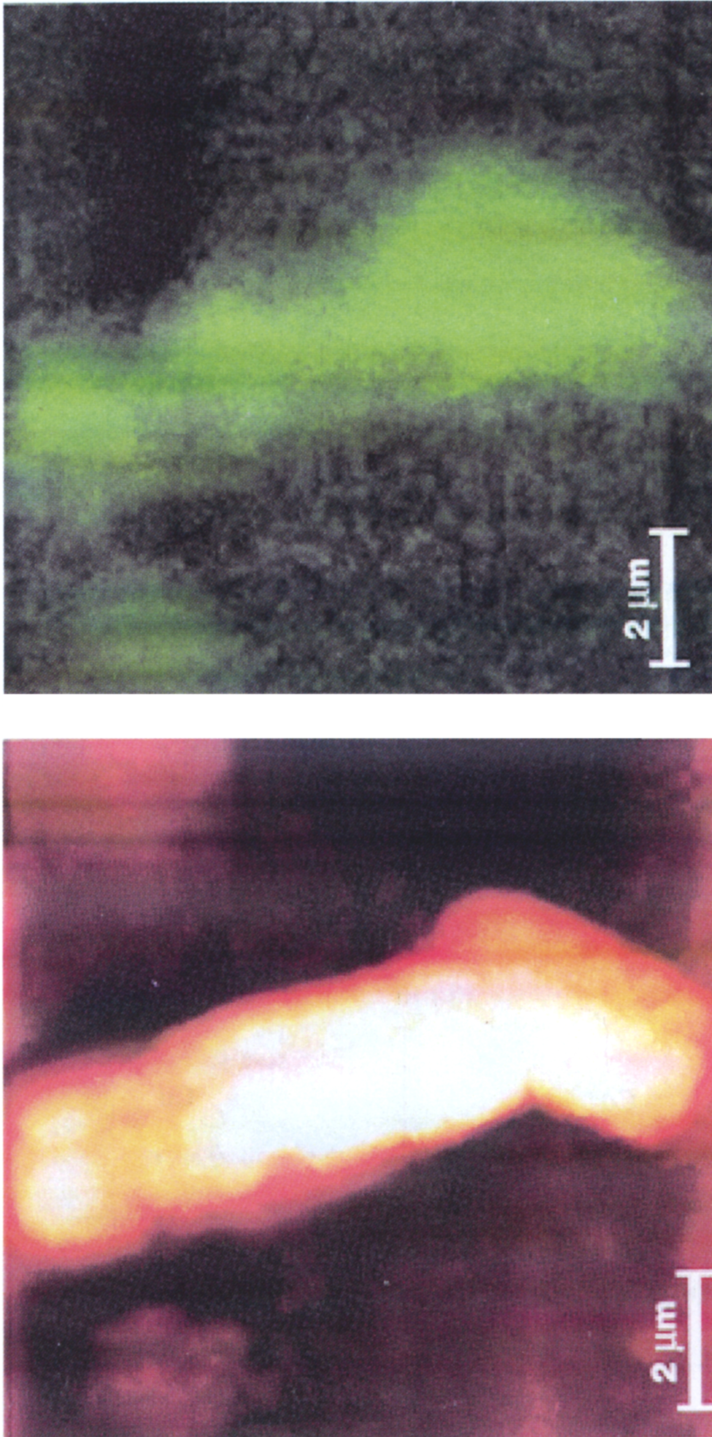

Figure 7. Images of green fluorescent protein bacterium. On the left is the AFM shear-force topographic image. The SNOM transmission image is on the right, clearly showing the capability of SNOM to identify functional groups (courtesy of Omicron Vakuumphysik, Germany).

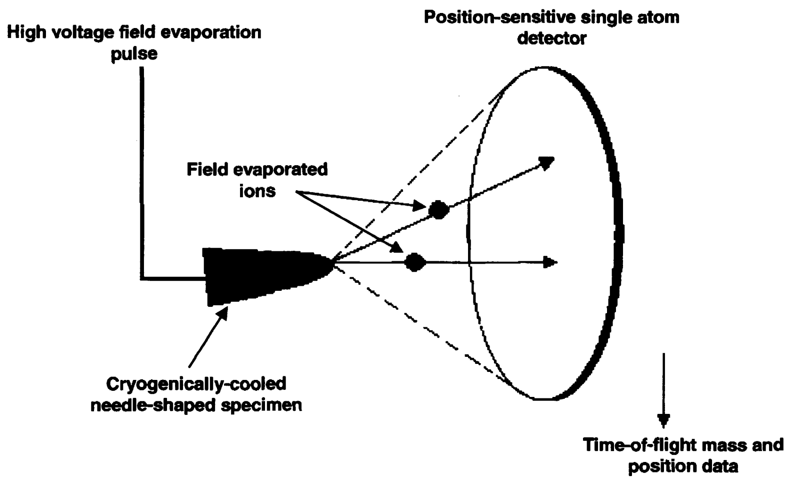

Figure 8. Schematic diagram of a 3-dimensional atom probe.

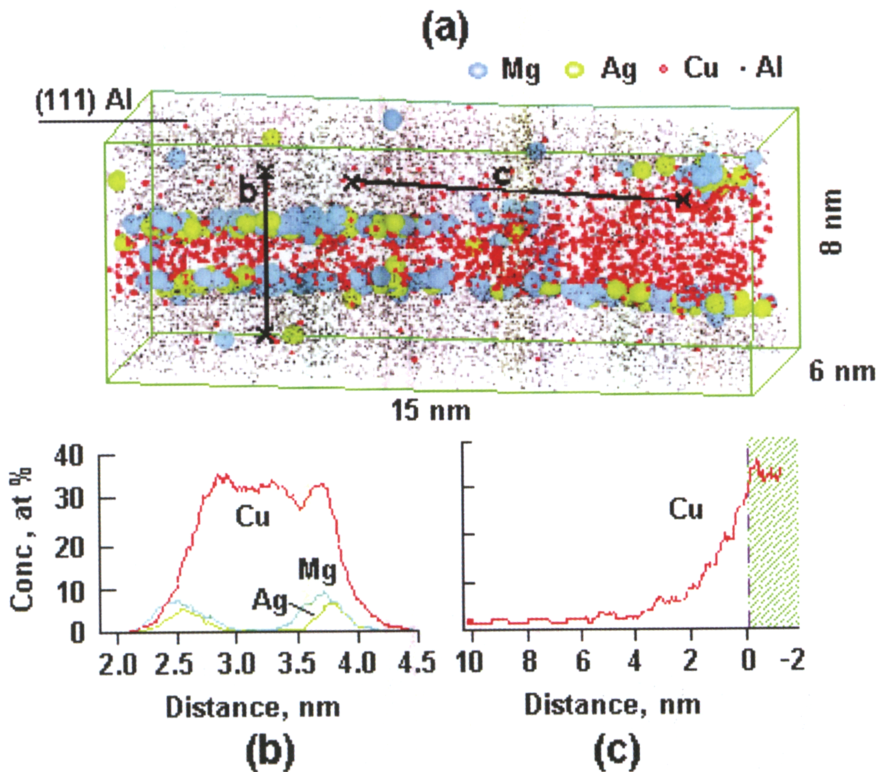

Figure 9. 3DAP elemental map of the omega (Ω) phase in an Al-1.9Cu-0.3Mg-0.2Ag alloy aged at 180°C for 10 hours. (a) is the concentration map; (b) and (c) are the concentration profiles obtained from the marked regions (courtesy of the National Research Institute of Metals, Japan).

3.3.6. Multifocal multiphoton microscopy

By producing an array of high aperture foci, multifocal multiphoton microscopy (MMM) provides real-time, light-efficient three-dimensional fluorescence imaging at high resolution, but without the need for a detection pinhole. This technique uses focused light from an ultrafast laser to produce light pulses of high peak intensity [121]. It creates and scans an array of focused spots, thereby reducing the scan time by a factor equal to the number of foci. The reduction of the distance between the foci increases not only the speed or image brightness but also the interference between neighboring focal fields given by the lens point-spread function. To overcome the interference effects, the MMM includes two transparent glass masks mounted onto a microlens array, each with a different pattern of holes. The optical path length through each microlens differs by greater than the laser pulse length making it possible to move the foci as close as 3.5 μm. This method is referred to as time multiplexing (TMX). Eventually, the interfocal distance can be reduced to the point that lateral scanning will not be needed.

The superior axial resolution of a TMX-MMM is illustrated by the images of a spiky pollen grain (30 μm) in Fig. 10. Without TMX, the *x-y* image shows significant haze (Fig. 10a). TMX removes the haze (Fig. 10b). The reconstructed three-dimensional images of the pollen grain also show similar improvement: the multiplexed image (Fig. 10c) exhibits much better definition than the 3-D image without multiplexing (Fig. 10d).

MMM (2- or 3-photon) has specific advantages compared to a confocal microscope:

- The excitation wavelength is longer;
- resolution is comparable to a confocal microscope without the need for a confocal pinhole, making optical alignment easier;
- more scattered light is collected which would be blocked by the pinhole in confocal microscopy;
- it scans up to 256 foci allowing much shorter acquisition times and increased image brightness; and
- foci can be aligned in a single line as close as 400 nm apart allowing *x*, *z*-scans or *x*, *y*-scans.

Potential applications of MMM relevant to particle imaging are listed below:

- Real-time 3D fluorescence microscopy on biological materials, including live cells;
- imaging kinetic phenomena involving metallic ions under different conditions;
- single particle tracking;
- biological cell manipulation;
- single molecule microscopy; and
- picosecond resolution microscopy and time-resolved imaging spectroscopy of particles.

3.3.7. Magnetic resonance force microscopy imaging

Magnetic resonance force microscopy (MRFM) is a rather new technique, whose ultimate goal is to image single electron spins [122-126]. This will make it possible to produce 3-dimensional, non-destructive, *in situ*, atomic-resolution images of atoms, molecules, defects in solids, dopants in semiconductors, and binding sites in viruses.

The method makes use of the very small forces between the magnetic moments of nuclei or electrons and a magnet. In a typical setup, a thin silicon cantilever is poised above a tiny sample containing the particle to be imaged. A magnetic particle mounted on the cantilever interacts with tiny volumes of magnetic atoms in the sample. By applying a high magnetic field gradient, a thin sheet of the sample is selected in which the magnetic moments are in resonance with an external rf-field. The magnetic field and the rf-field are modulated to generate a force at the mechanical resonance frequency of the cantilever. The MRFM device is operated in ultra-high vacuum and at liquid helium temperatures. This microscope uses beam deflection to detect sensor oscillations instead of interferometry in order to suppress tip-fiber interactions.

Estimates of the magnetic force exerted by a single electron range from 1 to 10 zN (1 zeptonewton (zN) = 10^{-21} N). Forces as small as 1.4 aN (1 attonewton (aN) = 10^{-18} N) have been detected to date [124].

3.3.8. Near-infrared Raman chemical imaging

A near-infrared Raman imaging microscope (NIRIM) has been recently developed to map chemical distribution on solid surfaces [127]. Since Raman spectroscopy is an inelastic light scattering process, it is very well suited to characterizing the chemical species on the surface of composite and biological materials. The major advantage of Raman imaging over other mapping techniques, such as SEM-EDS or SEM-WDS and AES or XPS, is that it can be performed under ambient conditions without the need for a high energy excitation source. The unique feature of the NIRIM is that it collects the entire multi-wavelength Raman spectra from each point in the illuminated area. This is accomplished by employing fiber-bundle image compression in which 100 fibers are arranged in a 10 × 10 square array. The resolution of the microscope is determined by the magnification of the objective and can be as small as the wavelength of the laser light ($\lambda \leq 1$ μm). The results from mapping of H_3BO_3 on B_4C and TiAlN on stainless steel showed good correlation with SEM-EDS analysis [128].

3.3.9. Near-field infrared atomic force microscopy

Scanning near-field microscopy has been extended into the infrared region of the spectrum [111-113] to obtain chemical information at 10-100 nm spatial resolution in nanomaterials and integrated circuits. In this method, the probe with a metallized AFM tip is operated in tapping mode, which extracts only the modulated part of the infrared radiation, while suppressing background light detection. Simultaneously, an IR beam (wavelength 10 μm) is focused on the AFM tip from

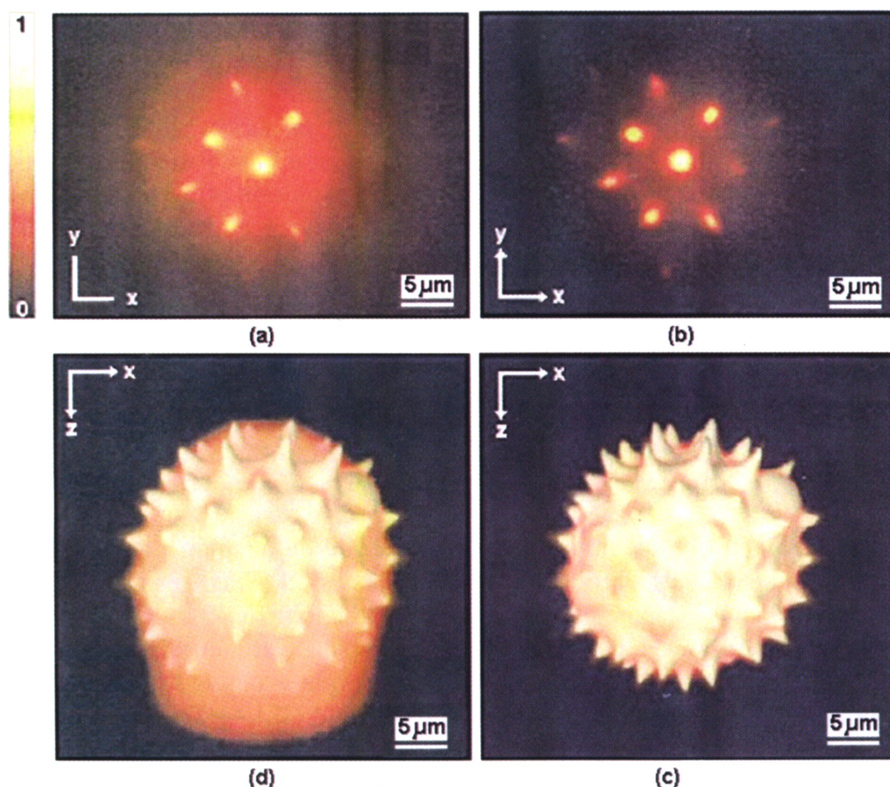

Figure 10. Effect of TMX on the 3D MMM image of a spiky pollen grain. Clockwise from top (a) *x-y* image shows significant haze; (b) TMX removes the haze; (c) reconstructed 3-D image with multiplexing; (d) reconstructed 3-D image without multiplexing (reprinted with permission from the Optical Society of America, cited in Ref. [121]).

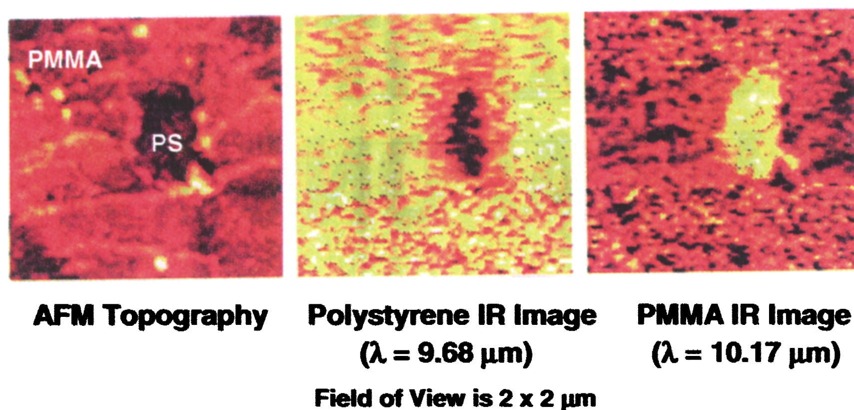

Figure 11. Surface topography (left) and IR absorption images of PS (middle) and PMMA (right) (courtesy of Max Planck Institut, Martinsried, Germany).

a tunable CO_2 laser. The light scattered from the metallized AFM tip is collected by a concave mirror and focused onto a detector. The changes in IR absorption at different laser wavelengths are measured while scanning the tip over the sample. The contrast between the sample components changes according to their relative absorption. For example, thin (15 nm) Au islands on a Si substrate appear bright, with a material contrast of 20-30% and a spatial resolution of 30 nm [112]. Similarly, the infrared contrast offered by vibrational resonance in a sample composed of two immiscible polymers (polystyrene (PS) embedded in a polymethyl methacrylate (PMMA) matrix) shows contrast reversal when the wavelength is changed from the absorption line of PS to the absorption line of PMMA (Fig. 11). The contrast is strongly enhanced in the near field of the Au probe tip, which is the first direct evidence of surface-enhanced infrared absorption.

4. SUMMARY

Recent developments in techniques for high-resolution imaging and characterization of nanometer-scale particles have been discussed. Single particle chemical composition analysis can be performed down at the ionic level by precision sizing and ionization followed by mass spectrometry of the ionized species. High-resolution (<1 Å) particle imaging techniques include scanning transmission electron microscopy with high angle annular dark field (HAADF) imaging. Atomic force and scanning tunneling microscopies have been successfully combined with analytical capabilities to provide chemical information at the nanoscale. Similar capability has been successfully demonstrated below 100 nm in scanning near-field optical microscopy (SNOM) combined with Raman, fluorescence and mass spectroscopies. A hot electron microcalorimeter-based EDS detector has the potential to provide significantly higher resolution X-ray analysis of particles than semiconductor energy-dispersive spectrometers.

REFERENCES

1. L.-H. Zhang and R. Koka, Data Storage **6(4)**, 15 (1999).
2. J.C. Vickerman (Ed.), *Surface Analysis: The Principal Techniques*, Wiley, New York, NY (1997).
3. G. Somorjai, in: *The New Chemistry*, N. Hall (Ed.), pp 137-166, Cambridge University Press, Cambridge (2000).
4. B. Fultz and J. Howe, *Transmission Electron Microscopy and Diffractometry of Materials*, Springer Verlag, Berlin (2001).
5. Z.L. Wang (Ed.), *Characterization of Nanophase Materials*, Wiley-VCH Verlag, Weinheim (2000).
6. W.M. Bullis, D.G. Seiler and A.C. Diebold (Eds.), *Semiconductor Characterization. Present Status and Future Needs*, AIP Press, New York, NY (1996).
7. D.G. Seiler, A.C. Diebold, W.M. Bullis, T.J. Shaffner, R. McDonald and E.J. Walters (Eds.), *Characterization and Metrology for ULSI Technology*, AIP Conference Proceedings No. 449, AIP Press, New York, NY (1998).
8. O. Preining, Pure Appl. Chem. **64**, 1679 (1992).

9. O. Preining, J. Aerosol Sci. **29**, 481 (1998).
10. K.E. Drexler, *Nanosystems*, Wiley, New York, NY (1992).
11. S. Sun, C.B. Murray, D. Weller, L. Folks and A. Moser, Science **287**, 1989 (2000).
12. T.T. Kodas and M.J. Hampden-Smith, *Aerosol Processing of Materials*, Wiley, New York, NY (1998).
13. W.C. Hinds, *Aerosol Technology*, 2nd Edition, Wiley, New York, NY (1999).
14. S.K. Friedlander, *Smoke, Dust and Haze: Fundamentals of Aerosol Dynamics*, 2nd Edition, Oxford University Press, New York, NY (2000).
15. R.W. Schoenlein, S. Chattopadhyay, H.H.W. Chong, T.E. Glover, P.A. Heimann, C.V. Shank, A.A. Zholents and M.S. Zolotorev, Science **287**, 2237 (2000).
16. V.A. Lobastov, R. Srinivasan, B.M. Goodson, C.-Y. Ruan, J.S. Feenstra and A.H. Zewail, J. Phys. Chem. A **105**, 1159 (2001).
17. A.H. Zewail, J. Phys. Chem. A **104**, 5660 (2000).
18. P.M. Paul, E.S. Toma, P. Breger, G. Mullot, F. Augé, Ph. Balcou, H.G. Muller and P. Agostini, Science **292**, 1689 (2001).
19. H. Niikura, F. Légaré, R. Hasbani, A.D. Bandrauk, M.Y. Ivanov, D.M. Villeneuve and P.B. Corkum, Nature **417**, 917 (2002).
20. R. Kienberger, M. Hentschel, M. Uiberacker, Ch. Spielmann, M. Kitzler, A. Scrinzi, M. Wieland, Th. Westerwalbesloh, U. Kleineberg, U. Heinzmann, M. Drescher and F. Krausz, Science **297**, 144 (2002). See also Nature **419**, 803 (2002).
21. A. Kaplan and P.L. Shkolnikov, Phys. Rev. Lett. **88**, 074801 (2002).
22. Y. Kousaka, T. Niida, K. Okuyama and H. Tanaka, J. Aerosol Sci. **13**, 231 (1982).
23. M.R. Stolzenburg and P.H. McMurry, Aerosol Sci. Technol. **14**, 48 (1991).
24. A. Wiedensohler, D. Orsini, D.S. Covert, D. Coffmann, W. Cantrell, M. Havlicek, F.J. Brechtel, L.M. Russell, R.J. Weber, J. Gras, J.G. Hudson and M. Litchy, Aerosol Sci. Technol. **27**, 224 (1997).
25. G.P. Reischl, Aerosol Sci. Technol. **14**, 5 (1991).
26. D. Chen and D.Y.H. Pui, J. Aerosol Sci. **26**, s141 (1995).
27. H. Fissan, D. Hummes, F. Stratmann, P. Buscher, S. Neumann, D.Y.H. Pui and D. Chen, Aerosol Sci. Technol. **24**, 1 (1996).
28. L. de Juan and J. Fernández de la Mora, J. Aerosol Sci. **29**, 589-599 (1998).
29. J. Fernández de la Mora, L. de Juan, T. Eichler and J. Rosell, Trends Anal. Chem. **17**, 328-339 (1998).
30. P.H. McMurry, Atmos. Environ. **34**, 1959 (2000).
31. M. Gamero-Castaño and J. Fernández de la Mora, J. Aerosol Sci. **31**, 757 (2000).
32. S.V. Hering and M.R. Stolzenburg, Aerosol Sci. Technol. **23**, 155 (1995).
33. J. Fernández de la Mora, S.V. Hering, N. Rao and P.H. McMurry, J. Aerosol Sci. **21**, 169 (1990).
34. J. Fernández de la Mora and A. Schmidt-Ott, J. Aerosol Sci. **24**, 409 (1993).
35. P.J. Ziemann, P. Liu, N.P. Rao, D.B. Kittelson and P.H. McMurry, J. Aerosol Sci. **26**, 745 (1995).
36. T. Seto, T. Nakamoto, K. Okuyama, M. Adachi, Y. Kuga and K. Takeuchi, J. Aerosol Sci. **28**, 193 (1997).
37. K.S. Seol, Y. Tsutatani, R.P. Camata, J. Yabumoto, S. Isomura, Y. Okada, K. Okuyama and K. Takeuchi, J. Aerosol Sci. **31**, 1389 (2000).
38. R.A. Fletcher and J.A. Small, in: *Aerosol Measurement: Principles, Techniques and Applications*, K. Willeke and P.A. Baron (Eds.), pp. 260-295, Van Nostrand Reinhold, New York, NY (1993).
39. R.A.W. Johnstone and C.G. Herbert, *Mass Spectrometry Basics*, CRC Press, Boca Raton, FL (2002).
40. L. van Vaeck, H. Struyf, W. van Roy and F. Adams, Mass Spectrom. Rev. **13**, 209 (1994).
41. W. Jambers, L. de Bock and R. E. van Grieken, Analyst **120**, 681 (1995).

42. R. Niessner, D. Klockow, F.J. Bruynseels and R.E. van Grieken, J. Environ. Anal. Chem. **22**, 281 (1985).
43. L.C. Wouters, R.E. van Grieken, R.W. Linton and C.F. Bauer, Anal. Chem. **60**, 2218 (1988).
44. F.J. Bruynseels, P. Otten and R.E. van Grieken, J. Anal. Atomic Spectrom. **3**, 237 (1988).
45. C.-U. Ro, I.H. Musselman and R.W. Linton, Anal. Chim. Acta **243**, 139 (1991).
46. D.M. Murphy and D.S. Thomson, Aerosol Sci. Technol. **22**, 237 (1995).
47. S.H. Wood and K.A. Prather, Trends Anal. Chem. **17**, 346 (1998).
48. C.A. Noble and K.A. Prather, Mass Spectrom. Rev. **19**, 248 (2000).
49. D. Knopf, P. Zink, J. Schreiner and K. Mauersberger, Aerosol Sci. Technol. **35**, 924 (2001).
50. H.J. Tobias, P.M. Kooiman, K.S. Docherty and P.J. Ziemann, Aerosol Sci. Technol. **33**, 170 (2000).
51. W.D. Reents and Z. Ge, Aerosol Sci. Technol. **33**, 122 (2000).
52. F. Li, T. Horvath, Z. Xie, T. Hoffmann and J.I. Baumbach, Int. J. Ion Mobility Spectrom. **4**, 100 (2001).
53. J.T. Jayne, D.C. Leard, X. Zhang, P. Davidovits, K.A. Smith, C.E. Kolb and D.R. Worsnop, Aerosol Sci. Technol. **33**, 49 (2000).
54. M. Yang, P.T.A. Reilly, K.B. Boraas, W.B. Whitten and J.M. Ramsey, Rapid Commun. Mass Spectrom. **10**, 347 (1996).
55. B. Warscheid and T. Hoffmann, Rapid Commun. Mass Spectrom. **16**, 496 (2002).
56. A.G. Harrison, *Chemical Ionization Mass Spectrometry*, CRC Press, Boca Raton, FL (1992).
57. D. Tanner, A. Jefferson and F. Eisele, J. Geophys. Res. **101**, 665 (1996).
58. W. Lindinger, A. Hansel and A. Jordan, Int. J. Mass Spectrom. Ion Processes **171**, 191 (1998).
59. T. Nordmeyer and K.A. Prather, Anal. Chem. **66**, 3540 (1994).
60. K.-P. Hinz, R. Kaufmann and B. Spengler, Aerosol Sci. Technol. **24**, 233 (1996).
61. E. Gard, J.E. Mayer, B.D. Morrical, T. Dienes, D.P. Fergenson and K.A. Prather, Anal. Chem. **69**, 4083 (1997).
62. D.M. Murphy, D.S. Thomson and M.J. Mahoney, Science **282**, 1664 (1999).
63. L. He and K.K. Murray, J. Mass Spectrom. **34**, 909 (1999).
64. M.A. Stowers, A.L. van Wuijckhuijse, J.C.M. Marijnissen, B. Scarlett, B.L.M. van Baar and Ch. E. Kientz., Rapid Commun. Mass Spectrom. **14**, 829 (2000).
65. P.T.A. Reilly, A.C. Lazar, R.A. Gieray, W.B. Whitten and J.M. Ramsey, Aerosol Sci. Technol. **33**, 135 (2000).
66. Z. Ge, A.S. Wexler and M.V. Johnston, J. Colloid Interf. Sci., **183**, 68 (1996).
67. K.R. Neubauer, S.T. Sum, M.V. Johnston and A.S. Wexler, J. Geophys. Res. **101**, 18701 (1996).
68. P.G. Carson, M.V. Johnston and A.S. Wexler, Aerosol Sci. Technol. **26**, 291 (1997).
69. K.R. Neubauer, M.V. Johnston and A.S. Wexler, Int. J. Mass Spectrom. Ion Processes **151**, 77 (1995).
70. D. Wollman, G.C. Hilton, K.D. Irwin, L.L. Dulcie, N.F. Bergren, D.E. Newbury, K.-S. Woo, B.Y.H. Liu, A.C. Diebold and J.M. Martinis, in: *Characterization and Metrology for ULSI Technology*, AIP Conference Proceedings No. 449, D.G. Seiler, A.C. Diebold, W.M. Bullis, T.J. Shaffner, R. McDonald and E.J. Walters (Eds.), pp. 799-804, AIP Press, New York, NY (1998).
71. K.D. Irwin, G.C. Hilton, J.M. Martinis and B. Cabrera, Nucl. Instrum. Methods Phys. Res. A **670**, 177 (1996).
72. A. Alessandrello, J.W. Beeman, C. Brofferio, O. Cremonesi, E. Fiorini, A. Guliani, E.E. Haller, A. Monfardini, A. Nucciotti, M. Pavan, G. Pessina, E. Previtali and L. Zanotti, Phys. Rev. Lett. **82**, 513 (1999).
73. L. Li, L. Frunzio, C. Wilson, D.E. Porter, A.E. Szymkowiak and S.H. Moseley, J. Appl. Phys. **90**, 3645 (2001).
74. G. Angloher, B. Beckhoff, M. Bühler, F. v. Filitzsch, T. Hertrich, P. Hettl, J. Höhne, M. Huber, J. Jochum, R.L. Mößbauer, J. Schnagl, F. Scholze and G. Ulm, Nucl. Instrum. Methods Phys. Res. A **444**, 214 (2000).
75. A. Fleischmann, T. Daniyarov, H. Rotzinger, C. Enns and G. Seidel, Preprint of paper presented at the 23rd International Conference on Low Temperature Physics, Hiroshima, Japan (August 2002).

76. K. Song, Y.-L. Lee and J. Sneddon, Appl. Spectrosc. Rev. **32**, 183 (1997).
77. D.W. Hahn and M.M. Lunden, Aerosol Sci. Technol. **33**, 30 (2000).
78. D. Anglos, Appl. Spectrosc. **56**, 2 (2001).
79. E. Tognoni, V. Palleschi, M. Corsi and G. Cristoforetti, Spectrochim. Acta B **57**, 1115 (2002).
80. L. Burgio, R.J.H. Clark, T. Stratoudaki, M. Doulgerides and D. Anglos, Appl. Spectrosc. **54**, 463 (2000).
81. D. Kossakovski and J.L. Beauchamp, Anal. Chem., **72**, 4731 (2000).
82. J. Liu, in: *Characterization of Nanophase Materials*, Z.L. Wang (Ed.), pp. 81-132, Wiley-VCH Verlag, Weinheim (2001).
83. K. Suenaga, M. Tencé, C. Mory, C. Colliex, H. Kato, T. Okazaki, H. Shinohara, K. Hirahara, S. Bandow and S. Iijima, Science **290**, 280 (2000).
84. P.E. Batson, N. Dellby and O.L. Krivanek, Nature **418**, 617 (2002).
85. M.A. O'Keefe, C.J.D. Hetherington, Y.C. Wang, E.C. Nelson, J.H. Turner, C. Kieselowski, J.-O. Malm, R. Mueller, J. Ringnalda, M. Pan and A. Thust, Ultramicroscopy **89**, 215 (2001).
86. P.E. Baston, Phys. Rev. B **61**, 16633 (2000).
87. S. Van Aert, A.J. den Dekker, A. van den Bos and D. Van Dyck, in: *Proc. IEEE Instrumentation and Technology Conference*, Budapest, Hungary, pp. 2081-2086, IEEE London (2001).
88. M.M.J. Treacy and S.B. Rice, J. Microscopy **156**, 211 (1989).
89. J. Liu and J.M. Cowley, Ultramicroscopy **34**, 199 (1990).
90. M.T. Otten, J. Electron Microscopy Techniques **17**, 221 (1991).
91. S.J. Pennycook, D.E. Jesson, A.J. McGibbon and P.D. Nellist, J. Electron Microscopy **45**, 36 (1996).
92. P.D. Nellist and S.J. Pennycook, Adv. Imag. Electr. Phys. **113**, 147 (2000).
93. E. Abe, H. Tarakura and A.P. Tsai, J. Electron Microscopy **50**, 187 (2001).
94. G.D. Danilatos, in: *In-Situ Microscopy in Materials Research*, P.L. Gai (Ed.), pp 14-44, Kluwer Academic Publishers, Dordrecht (1997).
95. Product Data Sheet for the XL30 ESEM-FEG Scanning Electron Microscope. FEI Company, Eindhoven (1998).
96. U.C. Fischer, in: *Scanning Probe Microscopy*, R. Wiesendanger (Ed.), pp. 161-210, Springer Verlag, Berlin (1998).
97. M. Ohtsu and H. Hori, *Near-Field Nano Optics*, Kluwer Academic Publishers, Dordrecht (1999).
98. N. van Hulst (Ed.), *6th International Conference on Near-Field Optics and Related Techniques*. J. Microscopy **202**, Parts 1 and 2 (April-May 2001).
99. T. Saiki and Y. Narita, Jpn. Soc. Appl. Phys. Int. **No.5**, 29 (January 2002).
100. E. Abbe, Arch. Mikroskop. Anat. **9**, 413 (1873).
101. G.A. Valaskovic, M. Holton and G.H. Morrison, Appl. Opt. **34**, 1215 (1995).
102. P. Hoffmann, B. Dutoit and R.-P. Salathé, Ultramicroscopy **61**, 165 (1995).
103. P. Lambelet, A. Sayah, M. Pfeffer, C. Philipona and F. Marquis-Weible, Appl. Opt. **37**, 7289 (1998).
104. Y.D. Suh and R. Zenobi, Adv. Mater. **12**, 1139 (2000).
105. K.C. Grabar, K.R. Brown, C.D. Keating, S.J. Stranick, S.-L. Tang and M.J. Natan, Anal. Chem. **69**, 471 (1997).
106. B.J. Kim, J.W. Flamma, E.S. ten Have, M.F. Garcia-Parajo, N.F. van Hulst and J. Brugger, J. Microscopy **202**, 16 (2001).
107. R. Eckert, J.M. Freyland, H. Gersen, H. Heinzelmann, G. Schürmann, W. Noell, U. Staufer and N.F. de Rooij, J. Microscopy **202**, 7 (2001).
108. P.N. Minh, T. Ono and M. Esashi (Eds.), *Fabrication of Silicon Microprobes for Optical Near-Field Applications*, CRC Press, Boca Raton, FL (2002).
109. F. Zenhausern, M.P. O'Boyle and H.K. Wickramasinghe, Appl. Phys. Lett. **65**, 1623 (1994).
110. S. Kühn, C. Hettich, C. Schmitt, J-Ph. Poizat and V. Sandoghdar, J. Microscopy **202**, 2 (2001).
111. B. Dragnea, J. Preusser, W. Schade and S.R. Leone, J. Appl. Phys. **86**, 2795 (1999).
112. B. Knoll and F. Keilmann, Nature **399**, 134 (1999).

113. B. Knoll and F. Keilmann, Opt. Commun. **182**, 321 (2000).
114. S. Webster, D.A. Smith and D.N. Batchelder, Vibrational Spectrosc. **18**, 51 (1998).
115. R. Zenobi, *Nanoscale Chemical Analysis & Spectroscopy*. Publication from the Zenobi Group, Analytical Chemistry Laboratory, ETH Zurich, Zurich (2002).
116. N. Hosaka and T. Saiki, J. Microsc. **202**, 362 (2001).
117. R. Stöckle, P. Setz, V. Deckert, T. Lippert, A. Wokaun and R. Zenobi, Anal. Chem. **73**, 1399 (2001).
118. A. Cerezo, T.J. Godfrey, S.J. Sijbrandij, G.D.W. Smith and P.J. Warren, Rev. Sci. Instrum. **69**, 1 (1998).
119. M.K. Miller, *Atom Probe Tomography. Analysis at the Atomic Level*, Kluwer Academic/Plenum Publishers, New York, NY (2000).
120. K. Hono, Acta Mater. **47**, 3127 (1999).
121. V. Andresen, A. Egner and S. W. Hell, Opt. Lett. **26**, 75 (2001).
122. D. Rugar, C.S. Yannoni and J.A. Sidles, Nature **360**, 563 (1992).
123. J.A. Sidles, J.L. Garbimi, K.J. Bruland, D. Rugar, O. Zuger, S. Hoen and C.S. Yannoni, Rev. Mod. Phys. **67**, 249 (1995).
124. D. Rugar, B.C. Stipe, H.J. Mamin, C.S. Yannoni, T.D. Stowe, K.Y. Yasumura and T.W. Kenny, Appl. Phys. A **72**, S3 (2001).
125. H. Kawakatsu, D. Saya, A. Kato, K. Fukushima, H. Toshiyoshi and H. Fujita, Rev. Sci. Instrum. **73**, 1188 (2002).
126. M.M. Midzor, P.E. Wigen, D. Pelekhov, W. Chen, P.C. Hammel and M.L. Roukes, J. Appl. Phys. **87**, 6493 (2002).
127. A.D. Gift, J. Ma, K.S. Habe, B.l. McClain and D. Ben-Amotz, J. Raman Spectrosc. **30**, 757 (1999).
128. K.N. Jallad, D. Ben-Amotz and A. Erdemir, Tribol. Trans. **45**, 239 (2002).